

Tuning the Optical Properties of Au Nanoclusters by Designed Proteins

Elena Lopez-Martinez, Diego Gianolio, Saül Garcia-Orrit, Victor Vega-Mayoral, Juan Cabanillas-Gonzalez,* Carlos Sanchez-Cano,* and Aitziber L. Cortajarena*

Gold nanoclusters (AuNCs) are nanomaterials with interesting photoluminescent properties that can be endowed with biomolecular recognition and biocompatibility when stabilized with proteins. The interplay between the optical features of AuNCs and the function added by the protein makes them perfect candidates for generating hybrid protein-inorganic nanomaterials. Focusing on protein stabilized-AuNCs, hitherto most of the work has covered the use of natural proteins for in situ growth of AuNCs. However, the exploitation of design proteins for such endeavors enables fine-tuning of the photoluminescent assets of AuNCs. In this work, rational protein engineering of modular protein scaffolds is applied for capping of non-emissive, non-passivated naked AuNCs, resulting in a fast and easy method for the synthesis of customizable and emissive protein-AuNC nanomaterials. Tuning of the photoluminescent properties of the final hybrid module is obtained by appropriate choice of the coordination residues grafted on the same protein scaffold. The effects of ligands and coordination bonds are studied using time-resolved photoluminescence and X-ray absorbance spectroscopies, shedding light on the mechanisms behind the emerging properties of these hybrid materials. Moreover, the described versatile strategy opens new avenues for the synthesis of on-demand photoluminescent hybrids for a wide spectrum of optical applications.


1. Introduction

Metal nanoclusters (NCs) are inorganic nanomaterials that have been widely used in sensing, biomedicine, and optics due to their interesting characteristics and outstanding optical properties. The features of the NCs are determined not only by their structure, such as the size dependent photoluminescence

(PL),^[1] but also by the ligands coordinated to them, as reported in recent studies.^[2] In this sense, the coordination of metal-NCs with biomolecules is an emerging area of research since this biomolecular capping can endow multiple capabilities to the NCs, including biocompatibility, stability in biological media, and biological functionality (e.g., binding and inhibitory functions) resulting in hybrid bio-nanomaterials with a plethora of potential applications.^[3]

In this context, it has been shown that the capping and stabilization of metal NCs with peptides and proteins affect the optical properties of the NCs and the interaction with living matter by means of specific biological interplay.^[4] Taking into account the role of the stabilizing agents on the NCs properties, an extra level of tailoring can be achieved by exploiting protein engineering. Metal coordinating engineered proteins are strongly inspired by natural metalloproteins, whose metal-binding capabilities allow to perform multiple functions, such as storage and transport,^[5,6] sensing,^[7,8] or catalysis.^[9,10] In this framework, designed repeat proteins emerged as an interesting option to display custom metal coordination sites. Repeat proteins can be used as building blocks due to their modularity, regular geometry, and small size; allowing the design of both simple, but also more complex supramolecular assemblies and multifunctional systems.^[11–14] The possibility of adding tailored chemical

E. Lopez-Martinez, C. Sanchez-Cano, A. L. Cortajarena
Center for Cooperative Research in Biomaterials (CIC biomaGUNE)
Basque Research and Technology Alliance (BRTA)
Paseo de Miramón 194, Donostia-San Sebastián 20014, Spain
E-mail: carlos.sanchez@dipc.org; alcortajarena@cicbiomagune.es

 The ORCID identification number(s) for the author(s) of this article can be found under <https://doi.org/10.1002/adom.202101332>.

© 2021 The Authors. Advanced Optical Materials published by Wiley-VCH GmbH. This is an open access article under the terms of the Creative Commons Attribution-NonCommercial-NoDeriv License, which permits use and distribution in any medium, provided the original work is properly cited, the use is non-commercial and no modifications or adaptations are made.

DOI: 10.1002/adom.202101332

D. Gianolio
Diamond Light Source Ltd
Harwell Science and Innovation Campus
Didcot, Oxfordshire OX11 0DE, UK
S. Garcia-Orrit, V. Vega-Mayoral, J. Cabanillas-Gonzalez
Madrid Institute for Advanced Studies
IMDEA Nanociencia
Calle Faraday 9, Madrid 28049, Spain
E-mail: juan.cabanillas@imdea.org
C. Sanchez-Cano, A. L. Cortajarena
Ikerbasque
Basque Foundation for Science
Plaza de Euskadi 5, Bilbao 48009, Spain
C. Sanchez-Cano
Donostia International Physics Center
Paseo Manuel de Lardizabal 4, Donostia-San Sebastian 20018, Spain

moieties on different protein modules expands the versatility of this tool. As a noteworthy example, consensus tetratricopeptide repeat (CTPR) proteins have been utilized as robust scaffolds for this purpose.^[15,16] CTPR units are small protein modules of 34 residues per repeat unit forming a helix-turn-helix structure. Long arrays of identical CTPR repeats fold in a right-handed superhelical structure in which 8 repeats form a complete superhelix turn. In previous works carried out in our group, engineered CTPR proteins with metal coordinating residues have been thoroughly employed for the in situ templating of photoluminescent NCs^[17,18] and quantum dots (QDs).^[19] Recently, the interest in tuning the photoluminescent properties of protein-coordinated metal NCs has yielded several works that assess the use of different amino acids and commonly used proteins as coordination agents.^[20,21] However, these works are focused on natural proteins, in which it is not possible to control the protein sequence and structure in a systematic manner. Therefore, up to now, there is no deep understanding of the role played by the coordinating protein on the features of NCs and the coupling between the protein structure and capping residues and PL properties of the cluster.

In this work, the aforementioned questions are tackled. The main aim of this study is to perform an exhaustive characterization of the behavior of metallic NCs scaffolded by engineered proteins. The approach selected to shed light on how the protein coordination affects the fluorescent properties of NCs, consists, on the one hand, on using gold nanoclusters (AuNCs) of identical characteristics capped with different ligands, and, on the other hand, using the same protein scaffold encoding different metal-coordinating residues at the same positions. Up to date, such a systematic approach to address this relevant aspect has not been reported. Towards this aim, a series of CTPR proteins were designed in which the metal-binding site is composed of different coordinating amino acids: either cysteines or histidines. Screening different amino acids coordinated to ex situ synthesized NCs will aim at deconvoluting the role of the capping ligands while avoiding the effects of metal coordinating residues on in situ NC growth. For the AuNC synthesis, the pioneering work by Prieto and co-workers,^[22] which described a method for the robust synthesis of water-dispersible AuNCs without organic ligands, so called naked gold nanoclusters (AuNKNCs), was applied. These non-passivated AuNCs, are non-emissive, and require subsequent coating with different small molecules such as adenosine monophosphate (AMP) or cysteines to achieve efficient PL in different spectral regions.^[22] Those naked NCs are therefore ideal for the proposed study by their conjugation with the two different coordinating designed proteins, which resulted in strikingly distinct emission properties. In this work, time-resolved PL spectroscopy and X-ray absorbance spectroscopies (XPSs) were deployed to study the photophysics of protein-AuNKNCs conjugates. The results of this work provide the first reported example of the simple generation of protein-NC systems with photophysical features tuned only by the protein template from a unique non-emissive nanomaterial. Most importantly, they contribute to an unprecedented understanding of the mechanisms behind the optical properties of metal nanomaterials when they are coordinated by biomolecules, in particular proteins.

2. Results and Discussion

CTPR proteins with different metal-coordination sites were designed based on the Protein Data Bank (PDB) crystal structure 2HYZ.^[23] Metal coordination sites consisting of a tetra-histidine (his) or a tetra-cysteine (cys) were engineered on a CTPR motif and then repeated 4 times in a tandem protein. These residues were chosen based on their ability to coordinate noble metals. The coordinating residues were introduced in positions 2, 6, 9, and 13 of the CTPR motif as previously described.^[24] Combining these mutated CTPR motifs (C_{4cys} or C_{4his} depending on the residue used for metal coordination), and the wild-type CTPR motif (WT) as flanking blocks, two proteins with six CTPR modules were constructed with the following structure: WT(C_{4his})₄WT and WT(C_{4cys})₄WT, which for the sake of clarity will be called C6-16his and C6-16cys respectively; each of these designed proteins include 16 coordinating residues (Figure 1). All the designed proteins contain an additional C-terminal solvating helix designed to improve the solubility in aqueous media with the inclusion of polar residues.^[25]

The AuNKNCs were synthesized following the protocol developed by Prieto and co-workers (see Experimental Section),^[22] resulting in a transparent solution of non-photoluminescent NCs of around 2 nm in size (Figure 2b,c). The AuNKNCs were washed to remove the excess reactants. The optical properties of AuNCs are one of their most valuable features. Different AuNCs can be synthesized in order to tune the emission properties and other spectroscopic features such as the PL lifetime. For example, the design of red-emitting clusters can be achieved with the capping of specific organic molecules (such as thiolates)^[26] or increasing the size of the NCs.^[27] The AuNKNCs-CTPR conjugates presented PL (Figure 2a), as expected considering the previous report in which capping AuNKNCs with organic molecules led to highly emissive systems. This result confirms the efficient coordination of AuNKNCs by the engineered proteins, whereas none of the controls, that is, CTPR WT protein without coordinating residues and CTPR-16glu protein with glutamic acids in the coordinating positions, led to emissive composites (Figure 2c and Figure S8, Supporting Information). Furthermore, the chemical identity of the metal coordinating amino acids (cys or his) within the protein encoded different emission color of the coordinated AuNKNCs when irradiated with a UV lamp (Figure 2a), and their absorbance spectra showed a tail in the 300–350 nm region (Figure 2b). Both protein-AuNKNCs systems displayed PL upon photoexcitation at 390 nm. The PL spectra of C6-16his-AuNKNCs (Figure 2c) peaks at 515 nm and tails down to 750 nm. Strikingly, the PL spectrum of C6-16cys-AuNKNCs peaks at 675 nm (Figure 2c) and tails down to 900 nm.

One of the parameters worth exploring is the coordination stoichiometry. Thus, the amount of AuNKNCs per protein in the conjugation reaction was varied from 3 to 100 molar excess of gold over protein. Since the increase in AuNCs size has an impact on the luminescent properties,^[27] we hypothesize that similarly, incrementing the number of effective coordinating residues bound to gold may also yield a PL change. Therefore, the Au stoichiometry was changed to explore a concomitant effect over the red and blue emission bands. The screening tests indicated that increasing the amount of gold per protein

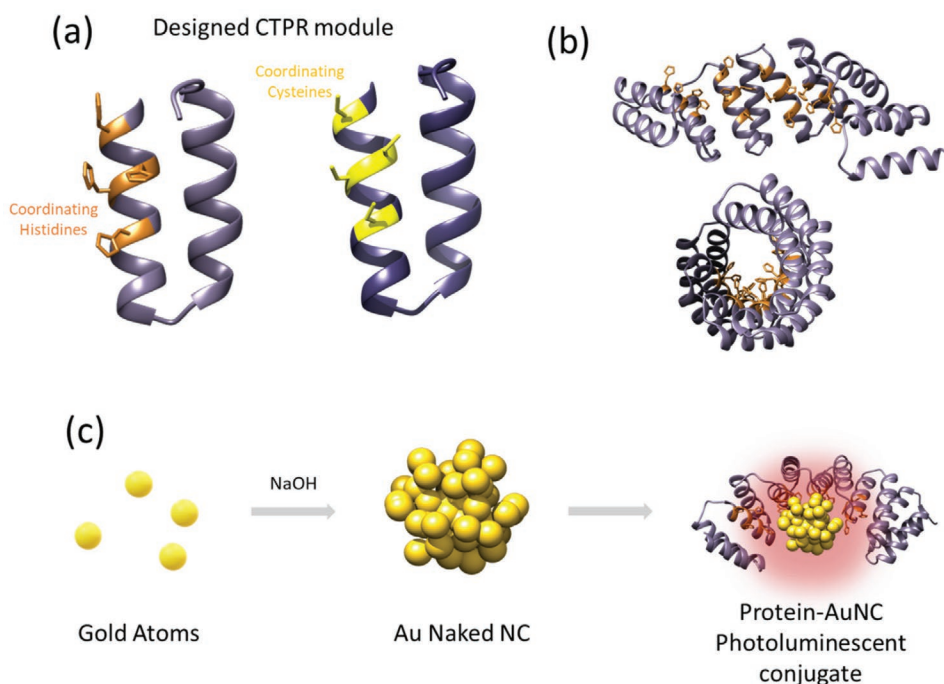


Figure 1. Designed CTPRs for the coordination of metal naked NCs. a) Mutated CTPR motif in which 4 metal-coordinating histidines (orange) are introduced at positions 2, 6, 9, and 13 within the 34 amino acid CTPR sequence. The same positions were mutated to 4 cysteines (yellow) for the construction of a coordinating protein module based on cysteines. b) 4 CTPR motifs with the metal-coordinating amino acids are combined and flanked with 2 wild-type CTPR modules to construct CTPR proteins with 6 repeats (C6-16cys and C6-16his). Front-view and side-view of C6-16his protein structural model based on the crystal structure of CTPR8 (PDB ID: 2HYZ).^[23] When the mutated CTPR units are combined with two WT capping repeats, the coordinating residues are localized on the inner concave surface of the CTPR superhelix. c) Scheme of the formation of CTPR-templated AuNKNCS, pre-formed Au naked NCs are coordinated by the engineered CTPR repeat proteins.

promoted the red emission band at the expense of the blue emission in C6-16cys-AuNKNCS, (Figure S1, Supporting Information). For the C6-16his-AuNKNCS only changes in PL intensity were observed, without significant spectral variations. Hereafter, an Au:protein molar ratio of 30 equivalents will be used, unless otherwise stated, since this ratio gives rise to the maximum PL intensity of C6-16his-AuNKNCS, bearing also a notable red emission contribution.

The protein-AuNKNCS conjugates were imaged using Transmission Electron Microscopy. The AuNKNCS grid presented gold nanoparticles with a mean diameter of 1.6 ± 0.3 nm (Figure S2,

Supporting Information) and similar polydispersity than that reported by Prieto and co-workers for naked NCs.^[22] After the conjugation, the purified protein-AuNKNCS conjugates showed a homogeneous dispersity consisting of a mean diameter of 1.7 ± 0.3 nm for C6-16cys-AuNKNCS and 1.7 ± 0.5 nm for C6-16his-AuNKNCS (Figure 3a), which is in agreement with the size obtained for the AuNKNCS and the previously reported molecule-capped AuNKNCS.^[22] The conjugates were further characterized using Matrix-Assisted Laser Desorption/Ionization-Time of Flight (MALDI-TOF) mass spectroscopy to confirm the coordination of AuNKNCS by the protein. The

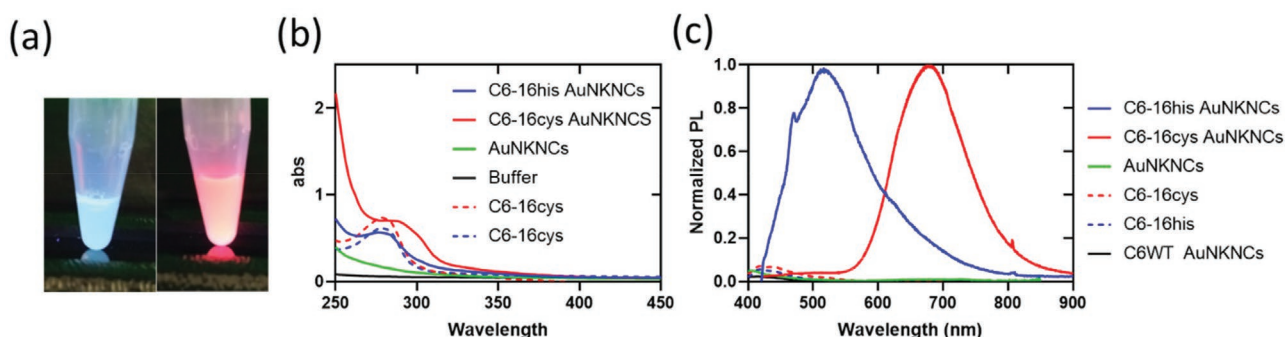


Figure 2. a) Picture taken on C6-16his-AuNKNCS (left) and C6-16cys-AuNKNCS conjugate liquid dispersions under UV light. b) Absorption spectra of AuNKNCS and protein-AuNKNCS conjugates: C6-16his-AuNKNCS, C6-16cys-AuNKNCS, C6-16his protein, C6-16cys protein, AuNKNCS, and buffer. c) PL spectra of C6-16his-AuNKNCS (solid blue), C6-16cys-AuNKNCS, C6-16his protein, C6-16cys protein, C6WT-AuNKNCS, and AuNKNCS upon photoexcitation at 390 nm. The spikes at 470 and 808 nm are ascribed respectively to buffer contribution and scattering from the pump.

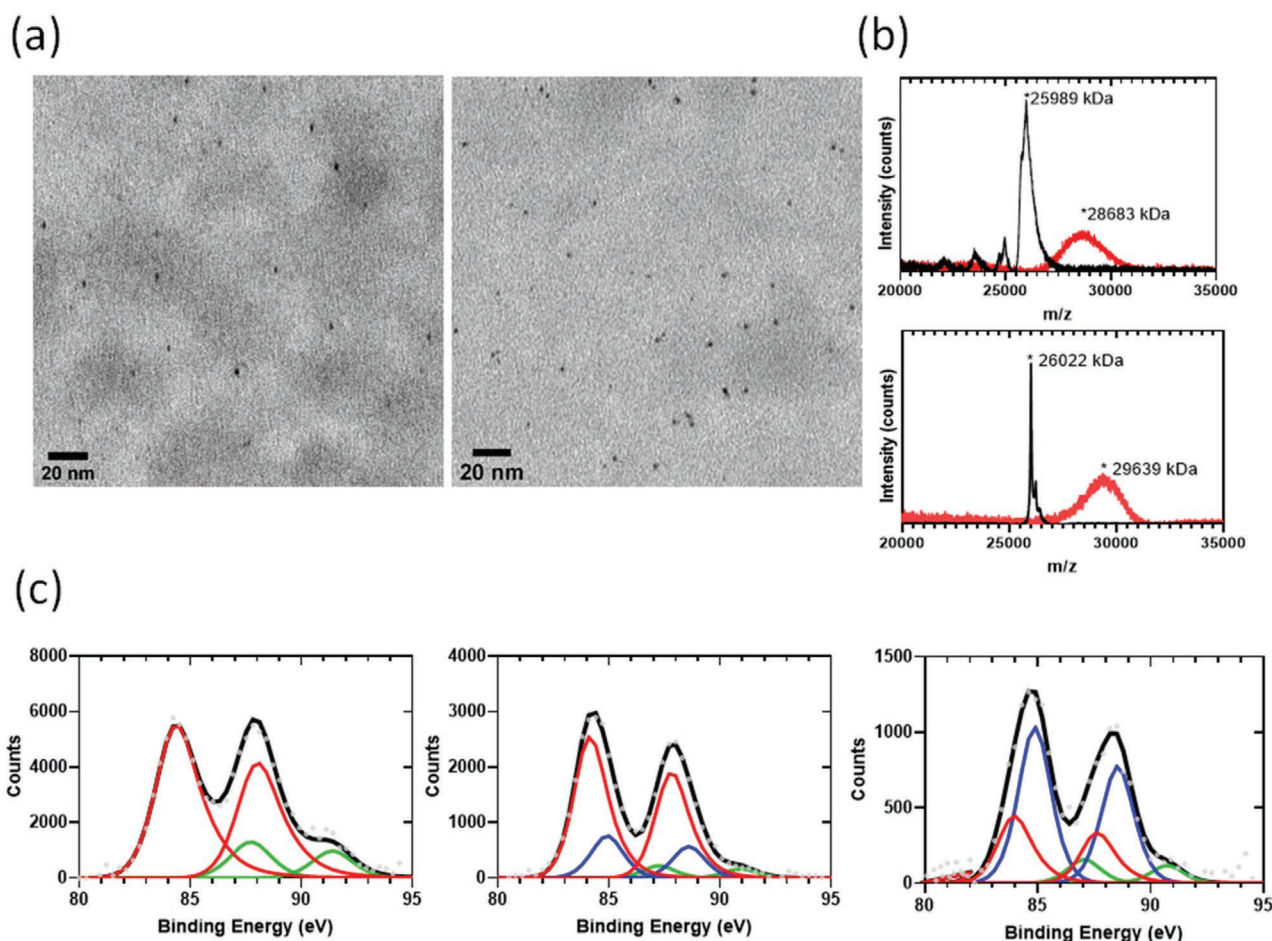


Figure 3. a) TEM micrographs at 120kV of the C6-16cys (left) and C6-16his (right) templated AuNKNs. The scale bar corresponds to 20 nm. b) MALDI-TOF mass spectra of the design proteins (black) and the protein-AuNKNs conjugates (red), for C6-16cys (top) and C6-16his (bottom). c) XPS spectra of AuNKNs (left), AuNKNs templated by C6-16cys (middle) and by C6-16his (right). The black lines correspond to the XPS spectra, and the colored lines correspond to the spectra deconvolution for the species Au(0) in red, Au(I) in blue, and Au(III) in green.

MALDI results showed that the mean size of metal NCs was 14 ± 7 gold atoms per cluster for the C6-16cys-AuNKNs conjugates and 18 ± 4 gold atoms per cluster for the C6-16his-AuNKNs (Figure 3b). Given the standard deviation of MALDI measurements, it is possible that the sample presents 18-gold atom clusters (among other populations). This is one of the so-called “magic numbers” for AuNCs and positively affects the robustness of the clusters since the 18-gold atom clusters have the exact number of electrons to fill the s, p, and d atomic orbitals.^[28] The conjugates were further characterized by X-ray Photoelectron Spectroscopy (XPS) in order to determine the oxidation state of the gold within the coordinated AuNKNs. The deconvolution of the signal of Au $4f_{7/2}$ showed a mixture of Au(0), Au(I), and Au(III) with binding energies at 84, 85, and 87.5 eV, respectively in both protein conjugates (Figure 3c). However, significant differences were observed in the relative ratios of the different oxidation states. For C6-16his-AuNKNs the relative amount of gold species was 27% Au(0), 63% Au(I), and 10% Au(III), while for C6-16cys-AuNKNs the relative amount of gold states was 72% Au(0), 22% Au(I), and 6% Au(III). This elemental analysis supports the fact that cysteine-

rich coordinating protein acts as a stronger reductant for gold than the histidine-rich protein. Moreover, the different ratios of gold species can be correlated with the optical properties of the coordinated clusters. In this respect, the Au(I) percentage of 22% on C6-16cys-AuNKNs agrees with the data reported in the literature for red-emitting thiolated-AuNCs,^[29] which usually ranges from 10 to 25%. Meanwhile, the higher binding energy observed on the Au $4f_{7/2}$ shell in C6-16his-AuNKNs is commonly described for blue-emitting AuNCs,^[30] related to the smaller size of the cluster as the binding energies increase.^[31] In the case of the standalone AuNKNs, the XPS analysis fitting revealed a composition of 80.5% Au(0) and 19.5% Au(III); which does not agree with the XPS data previously reported,^[22] consisting in a mixture of Au(0) and Au(I); probably due to the remaining Au(III) salts present in our AuNKNs sample.

In addition to steady-state PL (Figure 2c), time-resolved PL measurements were carried out in the protein-AuNKNs to shed light on their light-emitting properties. The PL dynamics of C6-16his-AuNKNs at 515 nm (Figure 4a,b) follow a three-exponential law with an amplitude-weighted average of 1.7 ns, whereas for C6-16cys-AuNKNs the PL at 700 nm decays

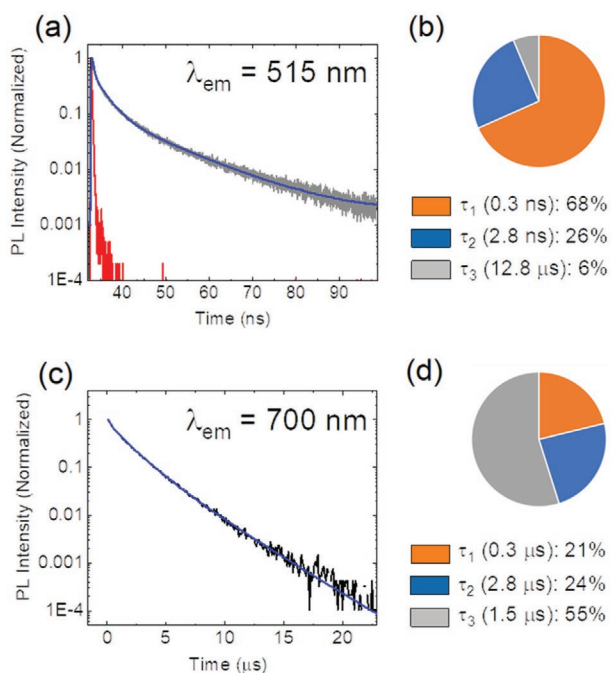


Figure 4. The PL decay curves of the protein-AuNKNCS conjugates. PL spectrum photoexcited at 405 nm, PL dynamics detected at the PL peak, and PL lifetime components obtained from a three-exponential fit of a,b) C6-16his-AuNKNCS and of c,d) C6-16cys-AuNKNCS. Blue lines in (a,c) stand for three-exponential fits to the PL decay curves. The red line in (a) represents the instrumental response function of the set-up.

slowly following a three-exponential law with an average lifetime of 1.6 μs (Figure 4c,d). In the case of protein conjugates produced with 100 equivalents of gold, the results depend on the type of protein functionalization. C6-16his-AuNKNCS possess two PL contributions at 515 and 700 nm, although its light emission is less intense than its 30 gold equivalents counterpart and C6-16cys conjugates. The PL at 515 nm decays with an amplitude average of 2.0 ns, whereas the PL band at 700 nm decays with an average lifetime of 0.9 μs , all of them following a three-exponential law. Contrarily, the PL spectrum of C6-16cys-AuNKNCS displays a maximum at 700 nm and PL decay following also a three-exponential model with an average lifetime of 1.2 μs (Figure S3, Supporting Information). The blue PL bands with nanosecond decay components are ascribed to AuNC inner transitions across the discrete levels within the Au d- and sp- bands, as reported elsewhere.^[32] The red PL band is in turn assigned to phosphorescence based on the associated microsecond PL decay and its strong intensity-dependence with oxygen (Figure S4, Supporting Information).

Taking into account that the protein conjugates were synthesized from a single batch of AuNKNCS, and thus their size should be the same, this difference in PL may not be a consequence of the NC size, as usually reported.^[1,27] Besides, the size inferred from the mass spectrometry results indicated that the blue-emissive histidine-coordinated AuNCs are only slightly larger than the red-emissive cysteine-coordinated AuNCs. Consequently, the change in the PL properties must instead be related to an interplay of the capping ligands on the AuNC electronic properties. The formation of ligand-to-

metal charge transfer (LMCT) or ligand-to-metal-metal charge transfer (LMMCT) states has been extensively described for ligand-capped AuNCs, especially those carrying thiol-Au coordination.^[33,34] The observed PL spectrum in C6-16cys-AuNKNCS conjugates is in accordance with previous reports in protein-templated AuNCs in which the coordination is achieved using cysteines,^[35,36] and also in AuNCs capped with small molecules using thiols.^[33,34] Furthermore, other bond-involved electron-rich heteroatoms and groups (O, N, -COOH, and -NH₂) have also been related to these mechanisms and could play an important role in the activation of the metal triplet state.^[37] In addition, as reported before, histidine-capped AuNCs hold a bluish-green emission (490 nm) with short lifetimes.^[38]

To further understand the role of the protein scaffold in the PL spectrum of the AuNKNCS and how the luminescence changes with a compromised protein structure, thermal denaturation ramp, and enzymatic digestion were performed. The experiments assess the protein secondary structure (thermal denaturation) and the primary integrity of the polypeptide chain (trypsin digestion). First, we performed circular dichroism spectrometry (CD) in order to check the protein integrity once the AuNKNCS were conjugated (Figure S5, Supporting Information). The results showed no significant change in the CD spectra for C6-16cys-AuNKNCS compared with the pristine protein. However, there was an evident change in the ratios between the minima at 220 and 205 nm in the histidine-rich protein, which points towards a partial loss of the alpha-helical content. When performing temperature ramps, the PL ($\lambda_{\text{ex}} = 390 \text{ nm}$) for C6-16cys protein conjugates did not change along the increasing temperature, while for the histidine-rich protein there was a significant increase in PL when the sample cooled down after the temperature ramp (Figure S6, Supporting Information). We hypothesize this could be due to a re-arrangement of the N–Au bond due to its less stiff nature when triggered by thermal movement.^[39] If this would be the case, a process of energy optimization could be the main cause of the emission increase observed. For C6-16cys-AuNKNCS conjugates, the rigidity of the S–Au bond could explain the absence of a significant change, since the restriction for internal molecular movements of such bonds could lead to emissive relaxation pathways when the cluster is excited.^[40,41] After trypsin digestion, a decrease in the emission intensity was observed but the remaining PL was maintained even at high concentrations of trypsin for both conjugates, although the protein was completely digested (Figure S7, Supporting Information), reinforcing the hypothesis about the importance of the surface ligand in PL, rather than the structural integrity of the protein. To further understand the role of the coordinating amino acids and the protein scaffold, controls in which the AuNKNCS were conjugated to L-cysteine and L-histidine were assessed using the same protocol and stoichiometry as for the protein conjugates. The samples were spectroscopically characterized using PL, UV–vis, and CD. They all lacked PL emission (Figure S8, Supporting Information), which points to the relevance of the protein metal-binding surface in the process of NC stabilization and tuning their optical properties.

The chemical and coordination properties of the NC in presence of the proteins were characterized using X-ray Absorbance Spectroscopy (XAS) to determine if there was a relation

between the chemical composition and coordination of the Au within the protein and the optical properties of the AuNCs. This experiment not only helps to corroborate the information about oxidation states obtained from XPS, but also becomes a useful tool to obtain information about the state of the clusters and the protein coordination.^[43,44] Protein-AuNCs conjugates were generated using both 30 and 100 equivalents of Au compared to the protein, concentrated to obtain solutions of at least 0.1 mg mL⁻¹ of gold, and studied at B18 beamline (Diamond Light Source). A number of controls were also analyzed, to determine possible changes in the AuNCs due to coordination to the proteins at residues different from the designed histidines or cysteines. These controls included non-passivated AuNCs, but also conjugates with two proteins with no specific gold coordinating residues: CTPR6 protein with 6 WT units (C6WT) and a CTPR with glutamic acids on the inner concave face (C6-16glu), which resulted in non-luminescent AuNCs, probably due to the interaction with other residues (i.e., lysines for C6-WT and glutamic acids for C6-16glu).

Principal Components Analysis (PCA) of the X-ray absorption near-edge structure (XANES) region of the spectra obtained (ranging from -20 to +80 eV around the edge) suggested the presence of 3 or 4 components on the set of samples measured. The standards used as components for the following Linear Combination Fitting (LCF) included: Au (0) foil; Au (III) hydroxide to mimic remaining Au salt; Au (I) Cl to emulate pos-

sible coordination of Cl to the NC during coordination to the proteins; Au (I) sulfide to reproduce coordination to cysteines; and Au (I) cyanide to model coordination to histidines, lysines or glutamic acids (as N, O, and C atoms are similar in size and better standards were not available).

Analysis of the individual samples using LCF (Figure 5, Table S1, Supporting Information) showed that AuNCs are mostly a combination of Au(0) and Au(III)OH. This result is in agreement with XPS analysis showing similar Au(0) and Au(III) populations, although in general XPS showed the presence of higher quantities of Au(0) in all of the samples measured. Yet, for both protein-AuNCs conjugates, Au(0) seems to disappear, being in disagreement with the data extracted by XPS (Table S1, Supporting Information). XANES analysis of C6-16cys-AuNCs conjugates suggested strong Au(I)-S coordination, and minor presence of other bonds (probably Au coordinated to nitrogen or oxygen), and a small percentage of Au(III) OH species. Equally, the binding of AuNCs to C6-16his seemed to be dominated by Au(I)-Cl or Au(I)-CN species probably indicating the coordination to nitrogen from the histidines. However, the analysis of C6-16his conjugates was more problematic due to the lack of a standard fully mimicking the Au-imidazole bond. Remarkably, the coordination of C6-16cys proteins with increasing amounts of AuNCs did not change, but greater amounts of Au(III) were observed when C6-16his was coordinated to 100 molar equivalents of gold. (Figure S9,

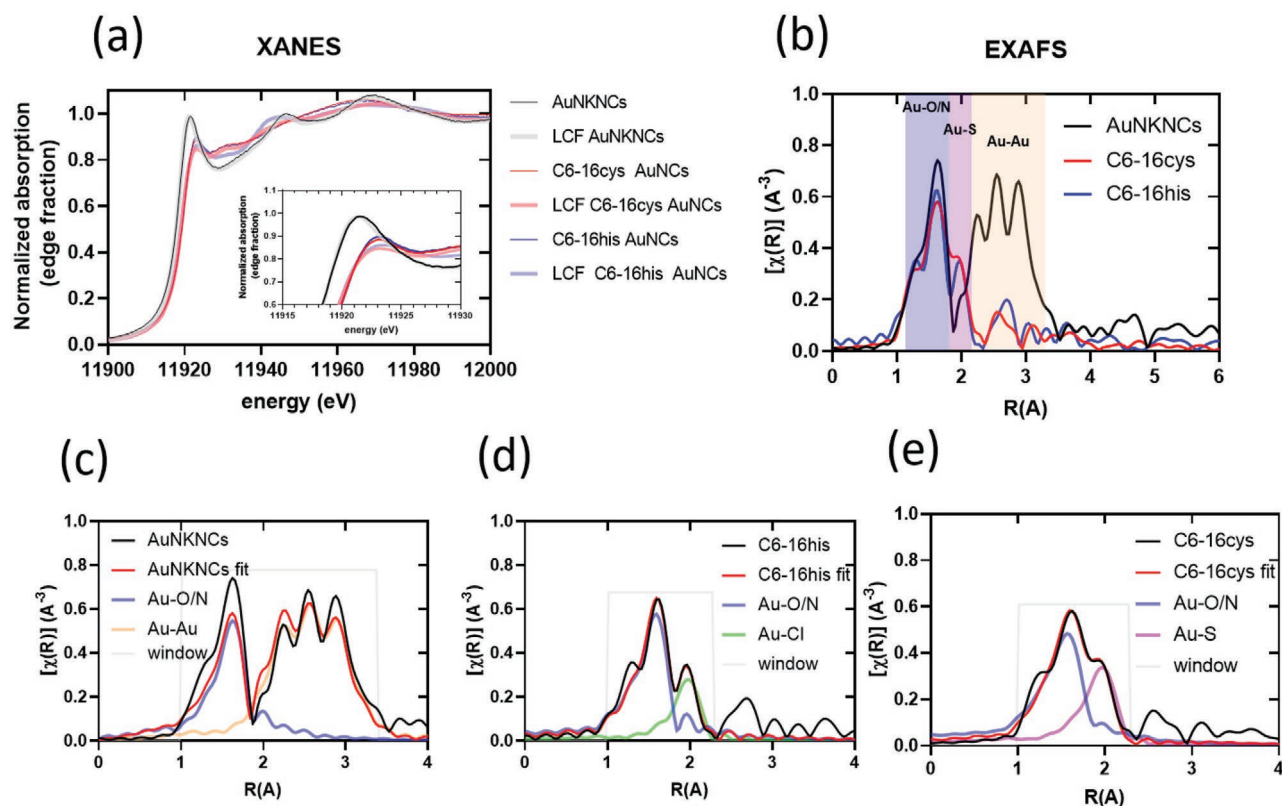


Figure 5. a) XANES spectra of the protein-AuNCs conjugates and their LCF: AuNCs (black, LCF in grey), C6-16cys-AuNCs (red, LCF in pale red), and C6-16his-AuNCs (blue, LCF in pale blue). Detail of the whiteline in the inset. b) FT-EXAFS of the AuNCs (black), C6-16cys-AuNCs (red), and C6-16his-AuNCs (blue), with the colored areas that correspond to the Au-O/N (blue), Au-S (purple), and Au-Au (orange) bonds. c-e) Fitted FT-EXAFS with the single path scattering analysis for each component of AuNCs (c), C6-16his (d), and C6-16cys (e) conjugates.

Supporting Information). The control proteins present different amounts of Au(I)-O/N species. Moreover, C6-16glu (a protein with glutamic acids at the coordinating positions) showed an Au(0) component in the fitting with increasing molar excess of gold. These data suggest that the presence of O or N from the glutamic acids and lysines can direct the coordination of gold, although their relative amount in the fitting is less determinant than in C6-16his (Table S1, Supporting Information). However, the coordination to glutamic acids and lysines did not translate into photo-emissive features, but in non-emissive coordination. Moreover, the results of XANES suggest a similarity between the coordination of metallic Au(0) in C6-16glu and the original non-emissive AuNKNCS; while C6-WT resembles the coordination seen in C6-16his conjugates.

Further analysis of the samples using extended X-ray absorption fine structure (EXAFS) allows obtaining information on the coordination sphere around the Au within the AuNCs, including the bond length and coordination numbers of the different bonds involved. Initially, LCF using the aforementioned standards was attempted to analyze the different samples (Figure S10, Supporting Information). However, the lack of standards fully mimicking the Au-imidazole (or other Au(I)-N/O bonds) made it difficult to obtain good fittings under these circumstances. Accordingly, analysis of the different samples was performed using only single scattering paths of the different types of Au bond expected (O, S, Cl, Au; where O includes both Au-O and Au-N contributions) for the fit (Figure 5). This analysis confirmed the main Au (0) character of AuNKNCS that was observed on XPS and XANES measurements. FT-EXAFS fitting in agreement with XANES suggested Au-Au coordination (bond length of 2.86 Å) for two-thirds of the Au in the NCs, while the other third of the gold was present in Au-O/N bonds (bond length of 1.99 Å).

FT-EXAFS also revealed interesting changes in the structure of AuNKNCS upon interaction with CTPR proteins. For example, analysis of the spectra from C6-16cys-AuNKNCS suggested the presence of both important Au-O/N and Au-S contributions in the structure of the clusters. Bond lengths for Au-O/N and Au-S were 1.98 and 2.32 Å, respectively. However, while the importance of Au-O/N in C6-16cys-AuNKNCS conjugates decreased when increasing amounts of AuNKNCS reacted with the protein, the contribution of Au-S to the structure of the AuNCs was not altered. Furthermore, the spectra of C6-16cys-AuNKNCS protein conjugates did not contain metallic contributions from Au-Au bonds commonly present in NPs and NCs with well-formed metallic cores. Equally, the FT-EXAFS spectra of C6-16his-AuNKNCS were mostly dominated by Au-O/N contributions (bond length 1.97 Å), and small amounts of Au(I)-Cl (bond length 2.32 Å; Table S2, Supporting Information), with no or little importance of Au-Au bonds (only a small contribution when the protein reacted with increasing amounts of AuNKNCS). Au-O/N contributions (bond length 1.99 Å) did also dominate the FT-EXAFS of control system C6WT-AuNKNCS, independently of the quantities of AuNKNCS used for the coordination to the protein. Still, a small peak between R 2.3–2.7 Å for samples containing both AuNKNCS and the WT protein, which is most likely a multiple scattering event, although it could also indicate possible Au...Au aurophilic interactions.^[44,45] Instead, C6-16glu-

AuNKNCS showed a combination of Au-O/N (bond length 1.94–1.98 Å) and large Au-Au single scattering contributions (bond length 2.83–2.84 Å). This suggested a strong Au(0) character for the NCs bound to those proteins. However, the size of the NCs when C6-16glu reacted with 30 or 100 equivalents of AuNKNCS are smaller than the unreacted ones, as estimated from the Amplitudes (S_0^{2*CN}) obtained from the FT-EXAFS fitting (Table S2, Supporting Information).

The evidence extracted from the EXAFS and XANES analysis points towards a change in the metallic character of the AuNKNCS, which is lost upon protein coordination with both types of his-based and cys-based CTPR protein scaffolds designed to bind to the NCs. The main component in AuNKNCS is Au-Au bond, with an amplitude (S_0^{2*CN}) of 71 (Table S2, Supporting Information), in agreement with a cluster core of metallic nature. In the case of the C6-16cys protein, the coordination is, as expected, predominantly directed by the sulfur present in the cysteines, although some Au-O/N coordination is also contributing, probably from few lysines and glutamic acids present in CTPR scaffolds. The lack of signals from Au(0) could relate to a coreless AuNC structure, such as Au-SR stapled catenanes, as reported previously on FT-EXAFS analysis of BSA-templated AuNCs.^[44] The interesting photoemission properties of Au(I)-thiolate structures have been extensively studied^[26,45] and rise as a good candidate for the type of cluster observed in C6-16cys-AuNKNCS. On the other hand, the coordination between C6-16his and AuNKNCS shows the main contribution from Au-O/N bonds. This is expected from the high amount of active nitrogen atoms in the protein, and together with a lack of realistic signals from Au-Au interactions should indicate the presence of Au-N stapled clusters. Besides, there is evidence pointing towards the stability and PL enhancement effect that N/O-containing groups such as amines or carboxylic acids have in photoluminescent protein-templated AuNCs^[33,37,46] and more importantly, the impact that amine-rich proteins have in shifting AuNCs PL towards blue.^[20] The glutamic acids present in the C6-16glu protein seem to be able also to direct the binding of AuNKNCS, but they do it without altering greatly their metallic nature (Table S2, Supporting Information), as observed by the presence of Au-Au interactions in C6-16glu samples, and the coordination numbers particle diameters estimated from the EXAFS spectra. Instead, the original CTPR scaffold (C6-WT) without any differential designed coordination residue displayed the expected general Au-O/N coordination, being representative of non-directed coordination, in opposition with the data extracted for the designed protein scaffold holding specific coordination residues geometrically tinkered alongside one verge of the protein.

XANES and EXAFS results combined with the PL studies suggest that the sole coordination by primary amine-containing or carboxylic groups on the WT and C6-16glu proteins, respectively, is not sufficient for an effective PL. In opposition, the PL observed in C6-16cys-AuNKNCS could rise from the interaction between the metal and thiols: LMCT and/or LMMCT transitions possibly due to the presence of new Au(I)-S bonds. Charge transfer from the sulfur to the Au(I) atom, most likely via a metal-centered triplet state, could explain the appearance of phosphorescence, manifested by an emission redshift and

long μs lifetimes.^[26,34] On the other hand, the high concentration in a reduced space of active imidazole groups in C6-16his-AuNKNs could compensate for the lack of a strong Au(I)-SR interaction, since imidazole can act as a coordinating group as well as a reductant. Moreover, the synthesized C6-16his-AuNKNs resemble histidine-capped AuNCs holding intense blue PL with lifetimes at the nanosecond regime.^[38,47] The Au(I)-N bond directed by the imidazole seems key to explain the fluorescent properties of C6-16his-AuNKNs, arising from optical transitions across the discrete molecular-like AuNC levels.

3. Conclusion

Protein-based AuNCs have risen as excellent biocompatible nanomaterials with valuable properties given by their PL and the molecular recognition capacities derived from proteins. Recently, the efforts put into comprehending the nature of the PL of such hybrids have shed light on the importance of ligands and synthesis conditions. Up to date these investigations, which represented the initial steps to study these relevant effects, were developed using natural and widely used proteins and peptides such as BSA, OVA, or GSH and in situ methodologies for the NC synthesis.

Herein, we have used the rational design on simple scaffolding proteins, CTPRs, to explore the effect of the coordinating protein on the PL properties of originally non-emissive AuNKNs by means of engineering specific coordination residues on the same protein scaffold. Additionally, the selection of previously described water-dispersible non-emissive AuNKNs allowed us to use the same nanomaterial to solely study the effect of the protein capping, without additional contributions of the coordination/reduction effects that the protein environment has on the in situ synthesis methods of metal NCs.

Besides, an extensive optical and X-ray spectroscopic characterization of the designed protein-AuNKNs composites sheds light on the mechanisms underlying the relationships between the NC composition and the metal coordination by biomolecules and optical properties of metal NCs. Interaction of unstabilized NCs with proteins carrying engineered strong metal coordination sites showed dramatic differences depending on the chemical nature of those amino acids. Proteins based on glutamic acid, a weak gold binder when compared with cysteines and histidines,^[48] maintained the metallic nature of the AuNKNs bond, and showed no PL. Yet, those carrying lysine, histidine, or cysteine transformed radically the structure of the clusters, losing their Au-Au metallic core and maybe being transformed into Au-N/S stapled type structures. These Au-amino acid interactions also seem to control the resulting photophysical properties of the clusters, allowing to switch and tune effectively the PL of clusters. In addition to the role of the coordinating residues on the PL properties, it was further demonstrated how constraining the cysteine and histidine metal-coordinating residues onto the hosting concave surface of the protein scaffold is key to enable PL, as the cluster coordination with monomeric amino acids did not result in photoluminescent complexes.

Finally, the reported synthesis method that combines engineered coordinating modules and naked NCs offers a quick, green, and easy way of developing emissive systems with tunable PL emission wavelengths and lifetimes.

With this work, we envision the asset of engineered repeat proteins as tailored, modular protein-based systems for the control interfacing of biomolecules with nanomaterials towards: 1) the fundamental physicochemical studies on the properties of emerging bio-nano hybrid materials with advanced properties, and 2) the design of future multifunctional protein-hybrids with customizing PL properties for a broad range of applications.

4. Experimental Section

Protein Expression and Purification: Proteins were over-expressed using *Escherichia coli* C41 cells. An overnight saturated cell culture was diluted and grown until the optical density reached 0.6 at 37 °C. At this point, the protein expression was induced using 0.6 mM of Isopropyl β -D-1-thiogalactopyranoside (IPTG) and the cells were grown at 30 °C for 5 h. Overexpressed proteins were purified using the His-tagged fusion method in a nickel nitriloacetic acid (Ni-NTA) affinity chromatography column, and His-tag removed using tobacco etch virus (TEV) protease. Then, electrophoresis gels were used to confirm the molecular weight and the purity of the purified proteins. The protein concentration was estimated using the molar extinction coefficient calculated from their amino acid composition. Purified proteins were stored at -80 °C.

AuNKNs Synthesis: The synthesis of the naked AuNKNs was developed by Prof. Prieto's laboratory.^[22] Briefly, AuNKNs were synthesized by mixing a NaOH solution (440 μL , 2M) with water (860 μL) and then adding an aqueous solution of HAuCl₄ (25 μL at 50 mM HAuCl₄; at a NaOH/Au molar ratio of 704/1). The mixture became colorless immediately and was kept without stirring for 1 h.

AuNKNs Conjugation to Proteins: Then the pH was adjusted using HCl and the protein was added in a molar ratio of 30/1 HAuCl₄/protein. The mixture was left overnight under stirring and covered from light. Then the sample was washed and concentrated using an Amicon 3 kDa ultrafiltration device. For the screening of conditions, the reagents and proteins were mixed in a microplate: AuNKNs were synthesized as mentioned before in situ in each well keeping the same molar ratios of gold and NaOH as exposed in the AuNKNs synthesis. After one hour, the protein was added to a final fixed concentration of 20 μM and left overnight. The PL was registered on a Biotek Synergy H1, with a λ_{ex} of 370 nm under aerobic conditions. The conditions tested were: presence or not of a reducing agent at 50 mM (dithiothreitol -DTT- and tris(2-carboxyethyl)phosphine-TCEP-, both purchased from Sigma Aldrich), and presence or absence of HCl (14 μL of stock solution at 2M in each well).

TEM Imaging: TEM measurements were conducted on JEOL JEM 1400 Plus microscope (120 kV). The samples for TEM were prepared by drop contact of the sample solution at 100 nM concentration of protein with a TEM grid and blotted to dry. The analysis of the images was performed using ImageJ software.

MALDI-TOF MS Analysis: Mass spectra were acquired on an UltrafleXtreme III MALDI ToF mass spectrometer with delayed extraction (Bruker) equipped with a pulsed N₂ laser ($\lambda = 337$ nm). MALDI-TOF sample preparation included 2 μL of the sample mixed with 2 μL of sinapic acid (matrix) in 50:50 water/acetonitrile with 0.01% trifluoroacetic acid (TFA). Then, 1 μL of the mixture was deposited onto the MALDI plate and allowed to air-dry. All mass spectra were acquired in positive reflection mode using delayed extraction with an average of 50–100 laser shots and an excitation voltage of 20 kV.

X-Ray Photoelectron Spectroscopy: XPS measurements were performed with a SPECS SAGE HR 100 spectrometer equipped with a 100 nm mean radius PHOIBOS analyzer and a non-monochromatic X-ray source (Mg K α line of 1253.6 eV energy and 250 W), placed perpendicular to the

analyzer axis and calibrated using the 3d5/2 line of Ag, with a full width at half maximum of 1.1 eV. All measurements were made in an ultrahigh vacuum chamber at a pressure of around 8×10^{-8} mbar. An electron flood gun was used to neutralize for charge. Measurements were conducted directly on dry deposited films. The analysis of spectra was done with CasaXPS 2.3.15dev87 software. Spectra were charge-corrected fixing the adventitious carbon C 1s at 284.8 eV.

Optical and Photophysical Spectroscopy: Absorbance spectra of protein-AuNKNs conjugates were acquired on a 96-well microplate using a Biotek Synergy H1 spectrophotometer. For time-resolved PL measurements, a 405 nm PDL 828 Picoquant Sepia laser, with a 50 ps pulse duration was employed as a photoexcitation source. The repetition rate was set at 10 MHz. The beam was mildly focused on the sample. PL measurements were carried out in solution in 2 mm optical path quartz cuvettes. Samples were purged with N₂ prior and stirred while measuring. A 420 nm long-pass filter was used to remove scattering from pump pulses. PL was collected with a pair of achromatic, convergent lenses (2" diameter and a focal of 7.5 cm) and sent to a SP2500 Acton Research spectrometer to select the desired spectral window in an N₂-cooled CCD (Princeton Instruments). Two different excitation/detection configurations were employed to monitor the nanosecond and microsecond time domains. PL decay measurements in the ns-time domain involved excitation with the 405 nm picosecond diode laser described above with a repetition rate of 10 MHz, and acquisition with a PicoQuant HydraHarp-400 time-correlated single-photon counting (TCSPC) system. Analogous measurements in the μ s-time-domain involved excitation with a 355 nm passively Q-switched Nd:YAG laser (TEEM Photonics; 0.3 ns pulse duration, at 269 Hz repetition rate) and acquisition with a TimeHarp 260 TCSPC board. PL spectra were acquired by filtering the desired wavelength with a spectrometer (SP2500, Acton Research), and detected with a Picoquant PMA Hybrid-Photomultiplier Assembly with a transit time spread of less than 50 ps. PL decay analysis was carried out with a Fluofit software (Picoquant). The phosphorescence origin of C6-16cys-AuNKNs emission was assessed bubbling the sample with O₂ and afterwards bubbling with N₂. Solutions were purged for 3 min.

Thermal Stability versus Photoluminescence Measurements: PL was measured in a Biotek Synergy H1 spectrophotometer conducting thermal denaturation ramp from 20 to 100 °C and from 100 to 20 °C every 10 °C, using a λ_{ex} at 390 nm. Secondary structure of the protein-AuNKNs conjugates was checked using circular dichroism on a spectropolarimeter Jasco J-1500, with a PM-539 detector and a 150W Xe arc excitation lamp. CD spectra from 260 to 180 nm were measured at 20 and 100 °C using a scanning speed of 200 nm min⁻¹ and 5 accumulations, a bandwidth of 5 nm, a data pitch of 0.2 nm, and a D.I.T of 0.5 s. For the thermal denaturation ramps, the CD signal was recorded at 220 nm using a JP Selecta Tectron Bio thermostat controller.

Trypsin Digestion: Protein-AuNKNs samples were incubated with increasing molar equivalents of trypsin from porcine pancreas (Sigma Aldrich, CAS 9002-07-7), from 10:1 (trypsin:CTPR conjugates) to 1000:1 in 10X increments, and were incubated for 1 h. PL of the protein-AuNKNs conjugates was measured on a Biotek Synergy H1 equipment at $\lambda_{ex} = 390$ nm. Polyacrylamide gel electrophoresis was performed in order to check the protein integrity after trypsin digestion, running the digested samples with incremental amounts of trypsin at 200 V.

X-Ray Absorbance Fine Structure (XAFS): X-ray Absorption Spectroscopy data were collected at B18 beamline at Diamond Light Source at Au L₃-edge (11919eV) using Cr-coated mirrors and Si111 monochromator. Samples were measured in liquid form inside plastic Eppendorf tubes, at concentrations over 0.1 mg mL⁻¹ of Au. Data collection was performed in fluorescence mode by means of a 36-element solid-state Ge detector positioned at 90 degrees with respect to the incoming beam. Energy scans were performed from 11 719 to 12 919 eV (k-range up to 16 Å⁻¹) with a constant energy step of 0.3 eV and a total acquisition time of ca. 3 min per scan. Scans were repeated from 50 to 100 times per each sample and then averaged (where the number of repetitions was selected depending on Au concentration and XAS signal). The resulting spectra were from the I_F/I₀ signal, which was measured by an ion chamber placed before

the sample and filled with ca. 70mbar of Argon and up to 1 atm He (resulting in absorption of ca 10% of the incoming beam).

The standards used contained a mixture of the expected oxidation states present in the AuNKNs and protein samples, as well as some of the possible ligands bound to the Au once coordinated to the inner interface of the proteins studied. In particular, those standards included: Au (0) foil; Au (III) hydroxide; Au (I) Cl; Au (I) sulfide; and Au (I) cyanide. Those standards were obtained from XAS standard database provided by Hephaestus software, while Au(I) Cl was measured experimentally at I14 beamline (Diamond). All of the measurements and standards were calibrated using corresponding Au foil scans for the alignment of the edge to 11 919 eV.

Data processing and analysis were then performed with Athena and Artemis software from Demeter package using IFFFIT code.^[49] Initially, PCA was run on the series of Au samples in XANES region (-20 to +80 eV around the edge), and target transform was applied on a series of Au standards (including Au (0) foil, Au (III) hydroxide, Au (I) chloride, Au (I) sulfide, and Au (I) cyanide) to confirm their presence as components in the samples measured. XANES LCFs were then performed in the range -20 to +80 eV around the edge using the standards mentioned above.

EXAFS fits were performed in k-range from 2.5 to 15.5 Å⁻¹, and R-range from 1 to 2.4 Å (when only first shell was fitted) or from 1 to 3.4 Å (when also Au-Au signal was included in case of a significant fraction of metallic gold). In absence of a 3d structure, only single scattering paths were used for the fit, including: Au-O/N, Au-Cl, Au-S, Au-Au. Most of the parameters were left free to be optimized by the fits but values obtained by the fit of Au standards were used as starting guesses when possible. However, Deby-Waller for Au-O/N was fixed to 0.002 Å⁻² as found from fit of the Au (III) hydroxide standard, the decision to fix it was due to its strong correlation to the amplitude parameter. E₀ was optimized to different values for different paths because they were representative of fractions of the sample where Au atoms were in different oxidation states. Coordination Numbers (CN) were left free to be optimized by the fit. This was obtained by using a single parameter for amplitude that represents the product of S₀²*CN.

Supporting Information

Supporting Information is available from the Wiley Online Library or from the author.

Acknowledgements

A.L.C. acknowledges support by the European Research Council ERC-CoG-648071-ProNANO and ERC-PoC-841063-NIMM; Spanish State Research Agency (PID2019-111649RB-I00 and PDC2021-120957-I00); and the Basque Government (Elkartek KK-2017/00008; RIS3-2019222005). E.L-M thanks the Spanish State Research Agency for the FPI grant (BES-2017-079646). C.S.C. thanks Gipuzkoa Foru Aldundia (Gipuzkoa Fellows program; grant number 2019-FELL-000018-01/62/2019) for financial support. J.C.G. acknowledges support by the Spanish State Research Agency (RTI2018-097508-B-I00), as well as support from the European Union structural funds and the Comunidad de Madrid through projects NMAT2D (S2018/NMT-4511) and FULMATEN-CM, "Ultra-rapid photonics for designing new materials and efficiently capturing energy" (Y2018/NMT-5028). IMDEA Nanociencia acknowledges support from the "Severo Ochoa" Programme for Centres of Excellence in R&D (MINECO, grant SEV-2016-0686). V.V.-M. acknowledges financial support from the regional government of Madrid "Atraccion del talento" program (2019-T2/IND-12737). S.G.-O. is grateful to the Spanish State Research Agency for a Ph.D. grant (FPI, PRE2019-09345). This work was performed under the Maria de Maeztu Units of Excellence Program from the Spanish State Research Agency -Grant No. MDM-2017-0720 (CIC biomaGUNE). The authors thank Remei Escudero Franch for her development of preliminary work, Dr. A. Aires for providing the control CTPR-16glu protein, and

Dr. Desire Di Silvio at CIC biomaGUNE for support with the acquisition X-ray photoelectron spectroscopy measurements. All synchrotron experiments were performed at the B18 Beamline (Diamond Light Source, Oxford) under proposal number SP23098 and in house measurements.

Conflict of Interest

The authors declare no conflict of interest.

Data Availability Statement

Research data are not shared.

Keywords

designed proteins, gold nanoclusters, hybrid nanomaterials, photoluminescent nanoclusters, repeat proteins, X-ray absorbance fine structure

Received: June 30, 2021

Revised: September 6, 2021

Published online:

- [1] J. Zheng, C. Zhou, M. Yu, J. Liu, *Nanoscale* **2012**, *4*, 4073.
- [2] Q. You, Y. Chen, *J. Mater. Chem.* **2018**, *6*, 9703.
- [3] A. Beloqui, A. L. Cortajarena, *Curr. Opin. Struct. Biol.* **2020**, *63*, 74.
- [4] M. Sarikaya, C. Tamerler, A. K. Y. Jen, K. Schulten, F. Baneyx, *Nat. Mater.* **2003**, *2*, 577.
- [5] P. Huang, P. Rong, A. Jin, X. Yan, M. G. Zhang, J. Lin, H. Hu, Z. Wang, X. Yue, W. Li, G. Niu, W. Zeng, W. Wang, K. Zhou, X. Chen, *Adv. Mater.* **2014**, *26*, 6401.
- [6] J. Zang, B. Zheng, X. Zhang, P. Arosio, G. Zhao, *J. Nanobiotechnol.* **2019**, *17*, 79.
- [7] A. Aires, E. Lopez-Martinez, A. L. Cortajarena, *Biosensors* **2018**, *8*, 110.
- [8] M. V. Romeo, E. López-Martínez, J. Berganza-Granda, F. Goñi-De-Cerio, A. L. Cortajarena, *Nanoscale Adv.* **2021**, *3*, 1331.
- [9] J. Gurruchaga-Pereda, V. Martínez-Martínez, E. Rezabal, X. Lopez, C. Garino, F. Mancin, A. L. Cortajarena, L. Salassa, *ACS Catal.* **2020**, *10*, 187.
- [10] J. Gurruchaga-Pereda, V. Martínez-Martínez, E. Formoso, O. Azpitarte, E. Rezabal, X. Lopez, A. L. Cortajarena, L. Salassa, *J. Phys. Chem. Lett.* **2021**, *12*, 4504.
- [11] T. Z. Grove, L. Regan, A. L. Cortajarena, *J. R. Soc., Interface* **2013**, *10*, 20130051.
- [12] S. H. Mejias, E. López-Martínez, M. Fernandez, P. Couleaud, A. Martin-Lasanta, D. Romera, A. Sanchez-Iglesias, S. Casado, M. R. Osorio, J. M. Abad, M. T. González, A. L. Cortajarena, *Nanoscale* **2021**, *13*, 6772.
- [13] D. Sanchez-deAlcazar, S. H. Mejias, K. Erazo, B. Sot, A. L. Cortajarena, *J. Struct. Biol.* **2018**, *201*, 118.
- [14] A. Aires, D. Maestro, J. Ruiz del Rio, A. R. Palanca, E. Lopez-Martinez, I. Llarena, K. Geraki, C. Sanchez-Cano, A. V. Villar, A. L. Cortajarena, *Chem. Sci.* **2021**, *12*, 2480.
- [15] J. López-Andarias, S. H. Mejías, T. Sakurai, W. Matsuda, S. Seki, F. Feixas, S. Osuna, C. Atienza, N. Martín, A. L. Cortajarena, *Adv. Funct. Mater.* **2018**, *28*, 1704031.
- [16] S. H. Mejías, J. López-Andarias, T. Sakurai, S. Yoneda, K. P. Erazo, S. Seki, C. Atienza, N. Martín, A. L. Cortajarena, *Chem. Sci.* **2016**, *7*, 4842.
- [17] P. Couleaud, S. Adan-Bermudez, A. Aires, S. H. Mejías, B. Sot, A. Somoza, A. L. Cortajarena, *Biomacromolecules* **2015**, *16*, 3836.
- [18] A. Aires, I. Llarena, M. Moller, J. Castro-Smirnov, J. Cabanillas-Gonzalez, A. L. Cortajarena, *Angew. Chem., Int. Ed.* **2019**, *58*, 6214.
- [19] A. Aires, M. Möller, A. L. Cortajarena, *Chem. Mater.* **2020**, *32*, 5729.
- [20] Y. Xu, J. Sherwood, Y. Qin, D. Crowley, M. Bonizzoni, Y. Bao, *Nanoscale* **2014**, *6*, 1515.
- [21] M. H. Griep, N. M. Bedford, *JPhys Mater.* **2020**, *3*, 045002.
- [22] P. Londoño-Larrea, J. P. Vanegas, D. Cuaran-Acosta, E. Zaballos-García, J. Pérez-Prieto, *Chem. - Eur. J.* **2017**, *23*, 8137.
- [23] T. Kajander, A. L. Cortajarena, S. Mochrie, L. Regan, *Acta Crystallogr., Sect. D: Struct. Biol.* **2007**, *63*, 800.
- [24] A. Aires, V. Fernández-Luna, J. Fernández-Cestau, R. D. Costa, A. L. Cortajarena, *Nano Lett.* **2020**, *20*, 2710.
- [25] E. R. G. Main, Y. Xiong, M. J. Cocco, L. D'Andrea, L. Regan, *Structure* **2003**, *11*, 497.
- [26] Z. Wu, Q. Yao, O. J. H. Chai, N. Ding, W. Xu, S. Zang, J. Xie, *Angew. Chem., Int. Ed.* **2020**, *59*, 9934.
- [27] J. Zheng, C. Zhang, R. M. Dickson, *Phys. Rev. Lett.* **2004**, *93*, 77402.
- [28] P. Pyykkö, *Nat. Nanotechnol.* **2007**, *2*, 273.
- [29] D. M. Chevrier, A. Chatt, P. Zhang, *J. Nurse Pract.* **2012**, *6*, 064504.
- [30] S. Xu, X. Lu, C. Yao, F. Huang, H. Jiang, W. Hua, N. Na, H. Liu, J. Ouyang, *Anal. Chem.* **2014**, *86*, 11634.
- [31] S. Peters, S. Peredkov, M. Neeb, W. Eberhardt, M. Al-Hada, *Surf. Sci.* **2013**, *608*, 129.
- [32] M. Zhu, C. M. Aikens, F. J. Hollander, G. C. Schatz, R. Jin, *J. Am. Chem. Soc.* **2008**, *130*, 5883.
- [33] Z. Wu, R. Jin, *Nano Lett.* **2010**, *10*, 2568.
- [34] Z. Luo, X. Yuan, Y. Yu, Q. Zhang, D. T. Leong, J. Y. Lee, J. Xie, *J. Am. Chem. Soc.* **2012**, *134*, 16662.
- [35] D. Selvan, P. Prasad, S. Crane, A. Abuhagr, R. Covington, K. Artyushkova, G. Ramakrishna, S. Chakraborty, *Analyst* **2019**, *144*, 3949.
- [36] J. Xie, Y. Zheng, J. Y. Ying, *J. Am. Chem. Soc.* **2009**, *131*, 888.
- [37] T. Yang, B. Shan, F. Huang, S. Yang, B. Peng, E. Yuan, P. Wu, K. Zhang, *Commun. Chem.* **2019**, *2*, 132.
- [38] X. Yang, M. Shi, R. Zhou, X. Chen, H. Chen, *Nanoscale* **2011**, *3*, 2596.
- [39] M. Gatchell, M. Goulart, L. Kranabetter, M. Kuhn, P. Martini, B. Rasul, P. Scheier, *Phys. Chem. Chem. Phys.* **2018**, *20*, 7739.
- [40] J. Mei, N. L. C. Leung, R. T. K. Kwok, J. W. Y. Lam, B. Z. Tang, *Chem. Rev.* **2015**, *115*, 11718.
- [41] K. Pyo, V. D. Thanthirige, K. Kwak, P. Pandurangan, G. Ramakrishna, D. Lee, *J. Am. Chem. Soc.* **2015**, *137*, 8244.
- [42] H. Wei, Z. Wang, J. Zhang, S. House, Y.-G. Gao, L. Yang, H. Robinson, L. H. Tan, H. Xing, C. Hou, I. M. Robertson, J.-M. Zuo, Y. Lu, *Nat. Nanotechnol.* **2011**, *6*, 93.
- [43] R. Yang, D. J. Morris, T. Higaki, M. J. Ward, R. Jin, P. Zhang, *J. Phys. Chem. C* **2018**, *122*, 22776.
- [44] D. M. Chevrier, V. D. Thanthirige, Z. Luo, S. Driscoll, P. Cho, M. A. Macdonald, Q. Yao, R. Guda, J. Xie, E. R. Johnson, A. Chatt, N. Zheng, P. Zhang, *Chem. Sci.* **2018**, *9*, 2782.
- [45] D. M. Chevrier, L. Raich, C. Rovira, A. Das, Z. Luo, Q. Yao, A. Chatt, J. Xie, R. Jin, J. Akola, P. Zhang, *J. Am. Chem. Soc.* **2018**, *140*, 15430.
- [46] B. Paramanik, A. Kundu, K. Chattopadhyay, A. Patra, *RSC Adv.* **2014**, *4*, 35059.
- [47] Y. Guo, X. Zhao, T. Long, M. Lin, Z. Liu, C. Huang, *RSC Adv.* **2015**, *5*, 61449.
- [48] Y. N. Tan, J. Y. Lee, D. I. C. Wang, *J. Am. Chem. Soc.* **2010**, *132*, 5677.
- [49] B. Ravel, M. Newville, *J. Synchrotron Radiat.* **2005**, *12*, 537.